Journal of Sound and Vibration (2002) **249**(1), 55–82
doi:10.1006/jsvi.2001.3831, available online at http://www.idealibrary.com on IDEAL®

A COMPARISON OF BIODYNAMIC MODELS OF THE HUMAN HAND–ARM SYSTEM FOR APPLICATIONS TO HAND-HELD POWER TOOLS

S. Rakheja, J. Z. Wu, R. G. Dong and A. W. Schopper

Engineering & Control Technology Branch, NIOSH, 1095 Willowdale Road, MS 2027, Morgantown, WV 26505, U.S.A.

AND

P.-É. Boileau

IRSST, 505 boul. de Maisonneuve West Montreal, Que., Canada H3A 3C2

(*Received* 15 *December* 2000, *and in final form* 29 *May* 2001)

The biodynamic response characteristics of various mechanical models of the human hand and arm system, reported in the literature, are evaluated in terms of their driving-point mechanical impedance modulus and phase responses. The suitability of the reported models for applications in realizing a mechanical simulator and assessment of vibration behavior of hand-held power tools is examined using three different criteria. These include the ability of the model to characterize the driving-point mechanical impedance of the human hand–arm system within the range of idealized values presented in ISO-10068 (1998); the magnitude of model deflection under a static feed force; and the vibration properties of the human hand and arm evaluated in terms of natural frequencies and damping ratios. From the relative evaluations of 12 different models, it is concluded that a vast majority of these models cannot be applied for the development of a mechanical hand–arm simulator or the assessment of dynamic behavior of the coupled hand–tool system. The higher order models, with three and four degrees of freedom, in general, yield impedance characteristics within the range of idealized values, but exhibit excessive static deflections. Moreover, these models involve very light masses (in the 1·2–4·8 g range), and exhibit either one or two vibration modes at frequencies below 10 Hz. The majority of the lower order models yield reasonable magnitudes of static deflections but relatively poor agreement with idealized values of driving-point mechanical impedance.

1. INTRODUCTION

Prolonged exposure to hand–arm vibration (HAV) has long been associated with a complex of vascular, neurological and musculoskeletal disorders, often referred to as hand–arm vibration syndrome (HAVS) among the operators of hand-held power tools [1–3]. The occurrence of HAVS and the rate of degeneration have been attributed to several physical and biodynamic factors, such as intensity, frequency and direction of HAV, duration and pattern of exposure, grip force and posture. The potential injury risks posed by the HAV have been related to intensity of vibration, expressed in terms of root sum of squared frequency-weighted rms accelerations, as evident from the dose–response relationship described in ISO-5349-1 [4].

0022-460X/02/010055 + 28 $35.00/0

The occupational health and safety risks associated with the operation of power tools have been further supported by many epidemiological studies [5]. The findings of epidemiological studies, and the relationship between potential injuries and the nature of HAV, have prompted a strong desire to develop effective methods for the assessment and attenuation of tool vibration. The characteristics of HAV generated by the operation of power tools are considered to be affected by the dynamics of the coupled hand–tool system. The vibration transmission characteristics of power tools and/or vibration attenuation mechanisms are thus invariably investigated in either the laboratory or the field involving human operators [6, 7]. Different test codes have been proposed to evaluate the relative vibration characteristics of different tools and vibration attenuation mechanisms in the laboratory under controlled conditions [8]. Owing to the complex nature of tool vibration and coupled hand–tool system dynamics, such assessment methodologies require repetitive measurements involving representative human subjects and test conditions. Such measurement-based methodologies are also known to pose considerable complexities in the data analysis due to inter- and intra-subject variabilities. In view of the expected contributions due to the dynamics of the operator's hand and arm, and the effects of many intrinsic and extrinsic variables, assessment methods that either eliminate or reduce the involvement of human operators are considered highly desirable.

The applications of mechanical equivalent or biodynamic models of the human hand and arm offer considerable potential to carry out assessments through both analytical and experimental analyses where the involvement of human subjects could be considerably reduced [9–11]. The hand–arm vibration (HAV) models, when integrated with the analytical model of a power tool, could permit efficient evaluations of the tool design factors and vibration attenuation devices. A number of biodynamic models of the human hand and arm have been proposed to study the vibration amplitude and power flow in the coupled hand, tool and work piece system; the potential performance benefit of vibration attenuation mechanisms; and to develop test rigs and hand–arm simulators for the assessment of vibration transmission performance of different tools [12–17]. Although these models have been developed over the past 30 yr, only minimal evidence exists on their applications for either analytical or experimental assessments [9, 10]. Similar efforts on biodynamic modelling of seated occupants exposed to whole-body vibration have evolved into development of effective models and construction of anthropodynamic manikins for analysis and testing of automotive and suspension seats [18, 19]. The lack of applications of HAV models may be partly attributed to wide variations among the reported biodynamics response data and test conditions employed in different studies [16, 17]. Although the validity of each model in predicting the biodynamic response acquired in the particular study has been well established, considerable differences should be expected among the various models, but these have not been specifically investigated.

The methodologies employed to identify the models and their parameters raise additional concerns regarding their suitability. The identifications based upon curve-fitting a target dataset do not represent a unique solution, and it is possible to realize a vast number of model parameter sets that would equally satisfy the target curve and a specified error criterion [21]. In this paper, the response characteristics of reported biodynamic models are evaluated and compared in an attempt to examine their suitability for the development of a hand–arm simulator and for their applicability to the analyses of coupled hand–tool systems. The relative evaluations are performed using a performance criterion based upon the free-vibration response characteristics, driving-point mechanical impedance (DPMI) modulus and phase, and deflection response under constant feed force.

2. BIODYNAMIC MODELS OF THE HUMAN HAND AND ARM

A number of mechanical equivalent models have been developed to characterize the biodynamic response characteristics of the human hand and arm under vibration, which can be described in terms of "through-the-hand–arm" and "to-the-hand" response functions. The "through-the-hand-arm" response function describes the transmission of vibration to specific segments of the hand and forearm. The "to-the-hand" biodynamic response function relates the motion at the hand–handle interface to the force at the driving point. This function has been the focus of most studies on biodynamic response characterization and model development, while "through-the-hand–arm" function has been addressed in only a few studies [22–24]. The dose–response relationship described in ISO-5349-1 [4] requires that the vibration exposure assessment be based upon the 8 h energy-equivalent acceleration total value measured at the hand–handle interface. A mechanical model and/or simulator, derived on the basis of "to-the-hand" biodynamic response function, could enable the evaluation of the interface acceleration. This review thus focuses on the models developed to describe the "to-the-hand" biodynamic response of the human hand and arm, which has been expressed as dynamic stiffness, mechanical impedance or apparent mass by articulating the interface motion in terms of position, velocity or acceleration respectively. Most studies, including ISO-10068 [17], however, have expressed the biodynamic response in terms of driving-point mechanical impedance (DPMI), given by

$$Z(s) = \frac{F_q(s)}{\dot{q}(s)}, \tag{1}$$

where Z is complex DPMI, $\dot{q}$ is velocity measured at the driving point, F_q is the driving force along the axis of motion, $s = \mathrm{j}\omega$ and ω is angular frequency of vibration.

The majority of the HAV models invariably comprise linear and time-invariant inertial, restoring and dissipative elements, and they do not represent the biomechanical properties of the human hand and arm. This may be attributed to complexities in identifying the properties of the human hand and arm, and the associated non-linearities. Furthermore, the reported models characterize the biodynamic behavior of the hand and arm under uncoupled vibration along three orthogonal axes (x_h, y_h, z_h) defined in ISO-8727 [25], and they are usually applicable under specific conditions of grip and push forces, arm position, body posture, and characteristics of vibration excitation. The reported HAV models may be classified into two broad groups on the basis of their structure: lumped- and distributed-parameter models. The lumped-parameter models, in general, are not related to the anatomical or physiological representation of the hand–arm system, although some investigators have suggested some vague relationships.

Only one study could be identified in which the hand and arm are represented by the distributed-parameter models, where the structure is derived from the anatomy [26]. The lumped-parameter models can be further represented by two subgroups based upon the properties of the lumped elements. The first subgroup comprises the models developed on the basis of linear stiffness and damping elements, assuming negligible influence of grip force and vibration intensity on the visco-elastic properties of the hand and arm. These include: the single-d.o.f. models, reported by Dieckmann [27], Reynolds and Soedel [28], and Abrams [29]; two-d.o.f. models proposed by Miwa *et al.* [30]; three-d.o.f. models proposed by Reynolds and Falkenberg [14, 15], Meltzer [31], Mishoe and Suggs [13], Daikoku and Ishikawa [12], and Gurram *et al.* [32]; and four-d.o.f. models developed by Reynolds and Falkenberg [14], and Gurram [33]. The second subgroup of models comprises linear but

grip-force-dependent parameters to characterize the grip-force dependence of the biodynamic response. The three- and four-d.o.f. grip-force-dependent models proposed by Mishoe and Suggs [13], Reynolds and Falkenberg [14, 15] and Gurram [33] would fall within this subgroup. Owing to the lack of adequate data on grip-force-dependent impedance characteristics and reported inconsistencies among the data derived under different magnitudes of grip force [16], these models are analyzed for a constant magnitude of grip force. Table 1 summarizes the parameters of the selected models together with the range of excitation frequency and magnitude considered.

2.1. DISTRIBUTED-PARAMETER HAV MODELS

Wood *et al.* [26] proposed distributed-parameter models of the hand and forearm, and the entire hand–forearm–upper arm system. The hand and forearm model was formulated by representing the radius and ulna bones by homogeneous flexural members with distributed mass (expressed as mass/unit length, ρ_1 and ρ_2 for radius and ulna bones respectively) and stiffness (expressed by the moduli, EI_1 and EI_2) parameters, as shown in Figure 1(a). The viscous effect of soft tissues surrounding the bones is characterized by linear damping distributed along the bones (ξ_1 and ξ_2). The effective lengths of the beams (L_1 and L_2) are taken as the distance between the elbow joint and center of the gripped handle. The wrist is thus considered as a part of the two beams. The arm beams are coupled with the driving point through lumped masses and visco-elastic representation of the tissue material of the hand, which are modelled as a Kelvin visco-elastic model comprising parallel combinations of stiffness and damping elements (k_1 and c_1; k_2 and c_2). The mass due to tissue material of the hand is represented by two lumped masses (m_1 and m_2) coupled with the radius and ulna bones. A distributed-parameter model of the total hand–arm system was also realized by integrating a single beam representing the upper arm humerus bone to the hand and forearm model.

The proposed model was analyzed to derive its impedance response under vibration along the y_h-axis alone, using the transfer matrix approach. The distributed damping was incorporated in the model by considering complex beam stiffness, $EI_i^*(i = 1, 2)$, given by

$$EI_i^* = EI_i\left(1 + \mathrm{j}2\xi_i \frac{\omega}{\omega_{1i}}\right), \quad i = 1, 2, \tag{2}$$

where ω_{1i} is the frequency of the fundamental vibration mode. The impedance was derived upon considering that the beams are hinged at the left end (indicated by "A") and allowing the velocity at the right end "B" ($\dot{q}_B$) to vanish, such that

$$Z(\mathrm{j}\omega) = \frac{F_A(\mathrm{j}\omega)}{\dot{q}_A(\mathrm{j}\omega)}, \tag{3}$$

where F_A and $\dot{q}_A$ are the force and velocity developed at the hinged end, "A" respectively. The model parameters were identified upon curve-fitting the laboratory-measured DPMI characteristics of two subjects: a light-weight subject and a subject with relatively heavier build. The DPMI data was acquired under y_h-axis vibration of 0·5 g r.m.s. acceleration in the 30–1000 Hz frequency range. The subject's elbow was supported on a molded elbow rest, while gripping a 25 mm diameter handle mounted on a vibration exciter with a specified grip force. The authors, however, do not report the magnitude of the grip force. Two sets of model parameters were identified for two subjects, where the masses due to tissue materials of the hand (m_1 and m_2) were considered to be zero. While the model of the

hand and forearm provided reasonable agreement with the measured data, the DPMI response of the total hand and arm model resulted in a poor fit.

Since the contributions of the upper arm to the "to-the-hand" biodynamic response are expected to be relatively small, the proposed model of the hand and forearm for a subject with heavier build is considered for analysis in this study. The DPMI characteristics derived from the formulations presented by Wood *et al.* [26], however, differed considerably from the values reported by the authors in both the modulus and phase. A detailed derivation of the DPMI function helped to identify a few errors (typographical nature) associated with the reported formulation of the model. This model derivation is presented in Appendix A and the reported model parameters are summarized in Table 1.

2.2. LUMPED-PARAMETER MODELS

All of the reported biodynamic models, with the exception of that reported by Wood *et al.*, [26], are of lumped-parameter type. These models range from single-d.o.f. linear models to four-d.o.f. non-linear models. The human hand and arm is a complex and continuous system, and a higher order model is believed to yield a more accurate prediction of biodynamic response of the human hand and arm. In all of the reported studies, the mechanical impedance characteristics of the hand and arm are evaluated in laboratories assuming the tool handle as a rigid body. The dynamic forces and moments generated by the tool are resolved into a force vector and a moment vector acting through and about the center of mass of the tool. The dynamic force vector at the tool handle is expressed by three orthogonal components acting independently along the three axes defined in ISO-8727 [25]. Assuming small displacements at the handle location, the dynamic response of the hand–arm system is considered to be uncoupled along its three orthogonal directions. The majority of the studies have thus proposed three different models applicable under vibration acting along the three independent axes. The parameters of the reported lumped-parameter models along each independent axis are characteristically derived from the measured "to-the-hand" biodynamic response using curve-fitting techniques. Multiparameter non-linear-programming-based optimization techniques have also been used to identify the model parameters by minimizing a weighted error function of the DPMI magnitude and phase response [21]. The structure of selected models, together with their identified parameters, are described below.

2.2.1. *One-and two-d.o.f. models*

Reynolds and Soedel [28] proposed three uncoupled single-d.o.f. mass-excited mechanical models to characterize the biodynamic response of the human hand and arm under vibration along three orthogonal axes in the 20–500 Hz frequency range. The models were derived on the basis of measured DPMI response under different hand and arm postures and grip forces. Although the study suggested that two- to three-d.o.f. models are required to describe the biodynamic behavior, a two-stage piecewise linear single-d.o.f. model with two sets of parameters applicable in two different frequency ranges was identified for each axis of vibration. The resulting mechanical equivalent model is illustrated in Figure 1(b). The DPMI response of the model along a particular axis of vibration can be derived from

$$Z(s) = ms + c + \frac{k}{s}. \tag{4}$$

TABLE 1

Summary of parameters and range of excitations for reported distributed-parameter and linear lumped-parameter models[†]

Investigator(s)	Axis of vibration	Grip force (N)	Model parameters	Frequency range	Vibration magnitude
Wood *et al.* [25]	y_h	NR[‡]	$m_1 = m_2 = 0$, $L_1 = L_2 = 0{\cdot}34$ m, $k_1 = 10$, $k_2 = 34$, $c_1 = 9$, $c_2 = 18$, $EI_1 = 3{\cdot}6\,\mathrm{Nm}^2$, $EI_2 = 3\,\mathrm{Nm}^2$, $\rho_1 = 3{\cdot}1$ kg/m, $\rho_2 = 0{\cdot}7$ kg/m	30–1000	0·5 g r.m.s. acceleration
Reynolds and Soedel [27]	x_h y_h z_h	4·5–13·3	$m = 0{\cdot}308$, $k = 7{\cdot}62$, $c = 67{\cdot}5$ ($20 \leqslant f \leqslant 73$ Hz); and $m = 0{\cdot}0219$, $k = 53{\cdot}8$, $c = 85{\cdot}6$ ($f > 73$ Hz) $m = 0{\cdot}191$, $k = 4{\cdot}7$, $c = 65{\cdot}5$ ($20 \leqslant f \leqslant 40$ Hz); and $m = 0{\cdot}0072$, $k = 14{\cdot}86$, $c = 35{\cdot}7$ ($f > 40$ Hz) $m = 0{\cdot}103$, $k = 3{\cdot}65$, $c = 39{\cdot}5$ ($20 \leqslant f \leqslant 100$ Hz); and $m = 0{\cdot}0095$, $k = 29{\cdot}6$, $c = 62{\cdot}9$ ($f > 100$ Hz)	20–500	NR[‡]
Miwa *et al.* [29]	y_h z_h	78·5	$m_1 = 0{\cdot}05$, $m_2 = 0{\cdot}3$, $k_1 = 15$, $c_1 = 50$ $m_1 = 0{\cdot}1$, $m_2 = 0{\cdot}8$, $k_1 = 130$, $c_1 = 250$	10–1000	0·2 g acceleration
Mishoe and Suggs [13]	x_h y_h z_h	27	$m_1 = 0{\cdot}004$, $m_2 = 0{\cdot}063$, $m_3 = 0{\cdot}354$, $k_1 = 12{\cdot}1$, $k_2 = 111{\cdot}9$, $c_1 = 643$, $c_2 = 217$ $m_1 = 0{\cdot}00081$, $m_2 = 0{\cdot}041$, $m_3 = 0{\cdot}943$, $k_1 = 1{\cdot}804$, $k_2 = 119{\cdot}4$, $c_1 = 110$, $c_2 = 54$ $m_1 = 0{\cdot}017$, $m_2 = 0{\cdot}023$, $m_3 = 0{\cdot}49$, $k_1 = 1{\cdot}518$, $k_2 = 112{\cdot}4$, $k_3 = 69{\cdot}7$, $c_1 = 159$, $c_2 = 102$, $c_3 = 102$	20–2000	0·707 g r.m.s. acceleration
Daikoku and Ishikawa [12]	x_h y_h z_h	33	$m_1 = 0{\cdot}0125$, $m_2 = 0{\cdot}281$, $m_3 = 2{\cdot}3$, $k_1 = 101$, $k_2 = 11{\cdot}5$, $k_3 = 1{\cdot}33$, $c_1 = 209$, $c_2 = 65{\cdot}3$, $c_3 = 70$ $m_1 = 0{\cdot}00792$, $m_2 = 0{\cdot}0271$, $m_3 = 1{\cdot}87$, $k_1 = 80{\cdot}2$, $k_2 = 2{\cdot}32$, $k_3 = 1{\cdot}37$, $c_1 = 39{\cdot}9$, $c_2 = 86{\cdot}2$, $c_3 = 5{\cdot}83$ $m_1 = 0{\cdot}00452$, $m_2 = 0{\cdot}211$, $m_3 = 0{\cdot}466$, $k_1 = 230$, $k_2 = 32.7$, $k_3 = 0{\cdot}404$, $c_1 = 124$, $c_2 = 65{\cdot}1$, $c_3 = 9{\cdot}26$	8–200	6·93 m/s^2 acceleration, 1·15 mm at 8 and 10 Hz
Reynolds and Falkenberg—three d.o.f. [15]	x_h y_h z_h	25·4	$m_1 = 0{\cdot}053$, $m_2 = 0{\cdot}210$, $m_3 = 1{\cdot}75$, $k_1 = 175$, $k_2 = 0{\cdot}175$, $k_3 = 78{\cdot}8$, $c_1 = 175$, $c_2 = 43{\cdot}5$, $c_3 = 350$ $m_1 = 0{\cdot}011$, $m_2 = 0{\cdot}526$, $m_3 = 0{\cdot}018$, $k_1 = 17{\cdot}5$, $k_2 = 0{\cdot}175$, $k_3 = 78{\cdot}8$, $c_1 = 87{\cdot}6$, $c_2 = 35$, $c_3 = 35$ $m_1 = 0{\cdot}053$, $m_2 = 0{\cdot}158$, $m_3 = 0{\cdot}018$, $k_1 = 298$, $k_2 = 0{\cdot}175$, $k_3 = 245$, $c_1 = 140$, $c_2 = 263$, $c_3 = 70{\cdot}1$	5–1000	NR[†]
Reynolds and Falkenberg—four d.o.f. [15]	x_h y_h z_h	25·4	$m_1 = 0{\cdot}0018$, $m_2 = 0{\cdot}088$, $m_3 = 0{\cdot}28$, $m_4 = 1{\cdot}75$, $k_1 = 1{\cdot}75$, $k_2 = 315$, $k_3 = 0{\cdot}175$, $k_4 = 175$, $c_1 = 525$, $c_2 = 298$, $c_3 = 42$, $c_4 = 35$ $m_1 = 0{\cdot}0018$, $m_2 = 0{\cdot}088$, $m_3 = 1{\cdot}4$, $m_4 = 0{\cdot}175$, $k_1 = 1{\cdot}75$, $k_2 = 88$, $k_3 = 0{\cdot}175$, $k_4 = 35$, $c_1 = 140$, $c_2 = 280$, $c_3 = 52{\cdot}5$, $c_4 = 17{\cdot}5$ $m_1 = 0{\cdot}0018$, $m_2 = 0{\cdot}158$, $m_3 = 0{\cdot}28$, $m_4 = 0{\cdot}0175$, $k_1 = 0{\cdot}175$, $k_2 = 880$, $k_3 = 0{\cdot}175$, $k_4 = 350$, $c_1 = 315$, $c_2 = 350$, $c_3 = 701$, $c_4 = 1{\cdot}8$	5–1000	NR[‡]

Gurram—three d.o.f. [32]	x_h y_h z_h	10, 25, 50	$m_1 = 0{\cdot}0012$, $m_2 = 0{\cdot}175$, $m_3 = 4{\cdot}1$, $k_{01} = 0{\cdot}1$, $k_{02} = 0{\cdot}1$, $k_{03} = 13{\cdot}2$, $c_1 = 761$, $c_2 = 37{\cdot}8$, $c_3 = 0{\cdot}8$, $k_{G1} = 0{\cdot}1$, $k_{G2} = 0{\cdot}1$, $k_{G3} = 4$, $c_{G1} = 3{\cdot}11$, $c_{G2} = 0{\cdot}45$, $c_{G3} = 0{\cdot}41$ $m_1 = 0{\cdot}0065$, $m_2 = 0{\cdot}274$, $m_3 = 3{\cdot}82$, $k_{01} = 8{\cdot}2$, $k_{02} = 0{\cdot}1$, $k_{03} = 556$, $c_1 = 77{\cdot}6$, $c_2 = 21$, $c_3 = 60{\cdot}2$, $k_{G1} = 693$, $k_{G2} = 0{\cdot}2$, $k_{G3} = 1420$, $c_{G1} = 0{\cdot}14$, $c_{G2} = 0{\cdot}56$, $c_{G3} = 340$ $m_1 = 0{\cdot}096$, $m_2 = 0{\cdot}3$, $m_3 = 3{\cdot}5$, $k_{01} = 0{\cdot}1$, $k_{02} = 2000$, $k_{03} = 0{\cdot}5$, $c_1 = 234$, $c_2 = 64$, $c_3 = 0{\cdot}5$, $k_{G1} = 10$, $k_{G2} = 95\,000$, $k_{G3} = 10$, $c_{G1} = 0{\cdot}1$, $c_{G2} = 1$, $c_{G3} = 10$	10–1000	Sine: 1–3 g peak; random: 0·2–0·7 m/s^2 r.m.s.
Gurram—four d.o.f. [32]	x_h y_h z_h	10, 25, 50	$m_1 = 0{\cdot}0325$, $m_2 = 0{\cdot}12$, $m_3 = 0{\cdot}865$, $m_4 = 3{\cdot}8$, $k_{01} = 3{\cdot}1$, $k_{02} = 0{\cdot}2$, $k_{03} = 2{\cdot}5$, $k_{04} = 2680$, $c_1 = 296$, $c_2 = 50{\cdot}5$, $c_3 = 2{\cdot}9$, $c_4 = 7500$ $k_{G1} = 146$, $k_{G2} = 0{\cdot}2$, $k_{G3} = 0{\cdot}2$, $k_{G4} = 3750$, $c_{G1} = 25{\cdot}2$, $c_{G2} = 2{\cdot}45$, $c_{G3} = 0{\cdot}69$, $c_{G4} = 365$ $m_1 = 0{\cdot}0059$, $m_2 = 0{\cdot}274$, $m_3 = 0{\cdot}21$, $m_4 = 3{\cdot}5$, $k_{01} = 16{\cdot}6$, $k_{02} = 1280$, $k_{03} = 0{\cdot}2$, $k_{04} = 1500$, $c_1 = 67{\cdot}8$, $c_2 = 1$, $c_3 = 19{\cdot}1$, $c_4 = 0{\cdot}566$ $k_{G1} = 212$, $k_{G2} = 1520$, $k_{G3} = 10$, $k_{G4} = 750$, $c_{G1} = 0{\cdot}36$, $c_{G2} = 245$, $c_{G3} = 0{\cdot}36$, $c_{G4} = 10{\cdot}7$ $m_1 = 0{\cdot}0827$, $m_2 = 0{\cdot}138$, $m_3 = 0{\cdot}758$, $m_4 = 3{\cdot}15$, $k_{01} = 1{\cdot}7$, $k_{02} = 1720$, $k_{03} = 0{\cdot}1$, $k_{04} = 5{\cdot}6$, $c_1 = 242$, $c_2 = 95{\cdot}5$, $c_3 = 106$, $c_4 = 105$ $k_{G1} = 8$, $k_{G2} = 14\,200$, $k_{G3} = 8$, $k_{G4} = 81$, $c_{G1} = 1{\cdot}52$, $c_{G2} = 2{\cdot}68$, $c_{G3} = 0{\cdot}6$, $c_{G4} = 32{\cdot}4$	10–1000	Sine: 1–3 g peak; random: 0·2–0·7 m/s^2 r.m.s.
ISO-10068—three d.o.f. [17]	x_h y_h z_h	25–50	$m_1 = 0{\cdot}0267$, $m_2 = 0{\cdot}486$, $m_3 = 3{\cdot}1$, $k_1 = 4{\cdot}37$, $k_2 = 0{\cdot}132$, $k_3 = 1{\cdot}565$, $c_1 = 207{\cdot}5$, $c_2 = 18{\cdot}93$, $c_3 = 9{\cdot}1$ $m_1 = 0{\cdot}0086$, $m_2 = 0{\cdot}356$, $m_3 = 3{\cdot}246$, $k_1 = 27{\cdot}1$, $k_2 = 0{\cdot}3$, $k_3 = 6{\cdot}415$, $c_1 = 68$, $c_2 = 51{\cdot}75$, $c_3 = 30{\cdot}78$ $m_1 = 0{\cdot}03$, $m_2 = 0{\cdot}662$, $m_3 = 2{\cdot}9$, $k_1 = 5{\cdot}335$, $k_2 = 299{\cdot}4$, $k_3 = 2{\cdot}495$, $c_1 = 227{\cdot}5$, $c_2 = 380{\cdot}6$, $c_3 = 30{\cdot}3$	10–500	based upon synthesis of reported data
ISO-10068—four d.o.f. [17]	x_h y_h z_h	25–50	$m_1 = 0{\cdot}0043$, $m_2 = 0{\cdot}105$, $m_3 = 0{\cdot}566$, $m_4 = 4{\cdot}3$, $k_1 = 88{\cdot}8$, $k_2 = 1{\cdot}5$, $k_3 = 0{\cdot}1$, $k_4 = 3{\cdot}99$, $c_1 = 678$, $c_2 = 185$, $c_3 = 23{\cdot}9$, $c_4 = 34{\cdot}9$ $m_1 = 0{\cdot}0091$, $m_2 = 0{\cdot}0544$, $m_3 = 1{\cdot}42$, $m_4 = 3{\cdot}62$, $k_1 = 0{\cdot}65$, $k_2 = 193$, $k_3 = 0{\cdot}65$, $k_4 = 1$, $c_1 = 115$, $c_2 = 147$, $c_3 = 8$; $c_4 = 1000$ $m_1 = 0{\cdot}019$, $m_2 = 0{\cdot}0947$, $m_3 = 0{\cdot}655$, $m_4 = 4{\cdot}29$, $k_1 = 300$, $k_2 = 68$, $k_3 = 199$, $k_4 = 2{\cdot}04$ $c_1 = 591$, $c_2 = 203$, $c_3 = 199$, $c_4 = 239$	10–500	based upon synthesis of reported data
ISO-10068—Beam [17]	x_h y_h z_h	25–50	$m = 2{\cdot}38$, $J = 0{\cdot}009$, $k_1^* = 1114$, $k_3^* = 4715$, $k_2^* = k_1 = k_3 \approx 0$, $k_2 = 307{\cdot}9$, $c_1 = 486$, $c_2 = 0$, $c_3 = 18970$, $l_1 = 0{\cdot}192$, $l_2 = 0{\cdot}488$, $l_3 = 0{\cdot}286$ $m = 5{\cdot}77$, $J = 0{\cdot}009$, $k_1^* = 289{\cdot}4$, $k_3^* = 72070$, $k_1 = k_3 = k_2 \approx 0$, $k_2 = 1636$, $c_1 = 141$, $c_2 = 0$, $c_3 = 7234$, $l_1 = 0{\cdot}384$, $l_2 = 0{\cdot}475$, $l_3 = 0{\cdot}4615$ $m = 5{\cdot}316$, $J = 0{\cdot}0099$, $k_1^* = 2\,773\,000$, $k_3^* = 6207$, $k_1 = 50{\cdot}16$, $k_2 = 4{\cdot}185$, $k_3 = k_2 \approx 0$, $c_1 = 107$, $c_2 = 0$, $c_3 = 257{\cdot}7$, $l_1 = 0{\cdot}2584$, $l_2 = 0{\cdot}0033$, $l_3 = 0{\cdot}1395$	10–500	based upon synthesis of reported data

† *Note*: All the mass, stiffness and damping values are expressed in kg, kN/m and Ns/m respectively. The grip-dependent parameters (k_{G1} and c_{G1}) are reported in N/m/N and Ns/m/N and mass moment of inertia of the beam is reported in kgm^2.

‡ Not reported.

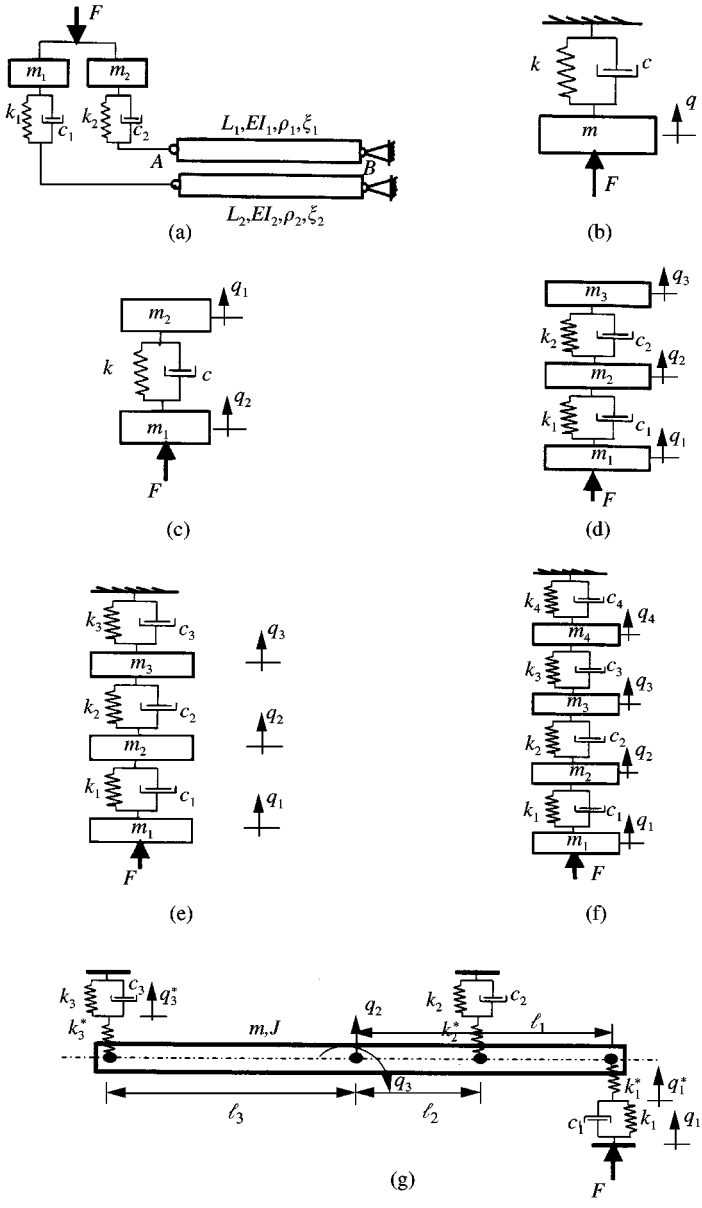

Figure 1. Schematics of mechanical equivalent models of the human hand and arm: (a) distributed-parameter model [26]; (b) single-d.o.f. model [28]; (c) two-d.o.f. semi-definite system model [30]; (d) three-d.o.f. semi-definite system model [30]; (e) three-d.o.f. models [12, 13, 15, 17, 33]; (f) four-d.o.f. models [14, 17, 33]; and (f) beam model [17].

Miwa *et al.* [30] proposed an equivalent electric circuit, whose series resonance corresponded to frequency corresponding to peak DPMI response of the hand and arm. The mechanical analogy of the proposed circuit is obtained as a mass-excited two-d.o.f. semi-definite system, shown in Figure 1(c). The model parameters were identified from the measured DPMI response under vibration along the compression (z_h) and shear (y_h) axes in the 10–1000 Hz frequency range, while the grip force was selected as 78·5 N. The DPMI

response of the proposed model under vibration along a particular axis was computed from

$$Z(s) = \frac{m_1 m_2 s^2 + s(m_1 + m_2)(c + k/s)}{m_2 s + c + k/s}. \tag{5}$$

2.2.2. *Three- and four-d.o.f. models*

Mishoe and Suggs [13] investigated the influence of grip force on DPMI characteristics of the human hand and arm. The measurements were performed under vibration along the three axes in the 20–2000 Hz frequency range using three different magnitudes of grip force: 13, 27 and 40 N. On the basis of measured data, three-d.o.f. semi-definite mechanical equivalent models were proposed to characterize the DPMI response under x_h- and y_h-axis of vibration. A three-d.o.f. model with fixed support characterized the DPMI response under z_h-axis of vibration. Figure 1(d) and 1(e) illustrate structures of the proposed mechanical equivalent models. Three sets of lumped parameters were identified to characterize the measured DPMI characteristics under three levels of grip force and each axis of vibration.

Daikoku and Ishikawa [12], Reynolds and Falkenberg [15], Gurram [33] and ISO-10068 [17] have presented a number of linear three-d.o.f. models, with structures identical to the z_h-axis model proposed by Mishoe and Suggs [13], shown in Figure 1(e). The parameters of these models, however, differ considerably. These differences can be attributed to two major factors. The first one is associated with differences among the laboratory-measured DPMI characteristics acquired in different studies, which are caused by dissimilar test conditions (grip force, vibration level, frequency range, type of excitation, posture, etc.) and variabilities among subjects employed in these studies. The second major factor is associated with the method of solution or parameter identification. It has been recognized that the identified model parameters do not represent a unique solution, and it is possible to realize a vast number of model parameter sets that would equally satisfy a measured DPMI target function or a specified error criterion. Gurram [33] employed a constrained multiparameter optimization to minimize a weighted function of both the magnitude and phase response in an attempt to improve the uniqueness of the solution. A set of limit constraints was defined to achieve model parameters within the known bounds. The total mass considered in the model was constrained to lie within the range of mean values of the human hand–arm system.

Owing to significant differences in the "to-the-hand" biodynamic response of human hand and arm reported by various investigators, a synthesis of selected data was performed based upon a proposed set of criteria considered to represent the most common range of test conditions [16]. These included a frequency range of 20–500 Hz, a grip force in the 25–50 N range and elbow angle close to 90°. The results of the study were used to identify the range of most probable values of DPMI. Based upon the mean values of the synthesized data, presented in ISO-10068 [17], a linear three-d.o.f. model of identical structure was also proposed.

The DPMI response characteristics of these models are derived from the solution of equations of motion, which may be expressed as

$$[M]\{\ddot{q}\} + [C]\{\dot{q}\} + [K]\{q\} = \{p\}, \tag{6}$$

where $[M]$, $[C]$ and $[K]$ are $(n \times n)$ mass, damping and stiffness matrices, respectively. The dimension n is the number of d.o.f. of the model. The $\{q\} = \{q_1, q_2, \ldots, q_n\}^{\mathrm{T}}$ and

$\{p\} = \{F, 0, 0, \ldots, \}^{\mathrm{T}}$ are $(n \times 1)$ vectors of mass displacement response and excitation forces, respectively, where superscript "T" designates the transpose.

Four-d.o.f. linear lumped-parameter models have also been proposed to characterize the "to-the-hand" biodynamic response of the human hand and arm [14, 17, 32]. The model structure is similar to that considered for three-d.o.f. models, as shown in Figure 1(f). The DPMI characteristics of the models are derived from a solution of the equations of motion, described in equation (6), such that

$$Z(s) = \frac{F(s)}{\dot{q}_1(s)}. \tag{7}$$

Some studies have attempted to relate some of the parameters and their variations to the physical visco-elastic behavior of the hand and arm. The mass m_1 of the three-d.o.f. model, shown in Figure 1(e), was considered to represent the mass of the cutaneous and part of the subcutaneous material that was in contact with the handle [15]. The parameter identification resulted in a very low value of this mass, which decreased further with increase in the grip force. The natural frequency associated with this mass was well in excess of 2000 Hz. Consequently, the dynamics of this mass was considered to be less important in view of the frequency range considered. This is further supported by results attained by Reynolds and Falkenberg [14, 15]. The high damping coefficient (c_1) located above m_1 indicated the possibility of dissipation of large amount of vibration energy in this contact region. For the four-d.o.f. model shown in Figure 1(f), the masses m_1 and m_2 have been attributed to mass due to dermis and epidermis, and the coupling elements, k_1 and c_1, are considered to represent the visco-elastic properties of these tissues. The strong coupling between the dermis and the subcutaneous tissue has been related to elements k_2 and c_2, while the mass m_2 is attributed to that of the subcutaneous tissue. The elements k_3 and c_3 are considered to represent weak coupling between the subcutaneous tissue and the muscle. The mass m_4 is thus believed to be representative of the hand muscle mass, while k_4 and c_4 relate to coupling between the muscle and the bones.

2.2.3. *Beam model*

A lumped-parameter beam model has also been proposed in ISO-10068 [17] to describe the "to-the-hand" biodynamic response of the human hand and arm under vibration along the three orthogonal axes. The structure of the model, which is identical along each axis, is illustrated in Figure 1(g). The model yields two coupled second order differential equations to describe the translational (q_2) and rotational (q_3) motions of a rigid beam of mass m and radius of gyration r, and three first order equations to describe the motions at the visco-elastic couplings (q_1^*, q_2^*, q_3^*). The equations of motion can be expressed in the matrix form of equation (6), where force input F is replaced by displacement excitation q_1 at the driving point. The equations are solved to compute the displacement response vector, and the DPMI characteristics of the model are then derived from

$$Z(s) = \frac{k_1 + sc_1}{s}\left[\frac{q_1^*}{q_1} - 1\right]. \tag{8}$$

An examination of the parameters presented in ISO-10068 [17] reveals that stiffness elements k_2 and k_2^* are negligible. This suggests that the model can be considered as a beam supported on its two ends and hinged at a point within its span.

2.3. GRIP-FORCE-DEPENDENT MODELS

It has been established that DPMI response of the hand–arm system is strongly dependent upon magnitude of the grip force [13, 33–36]. The linear lumped-parameter models, within the first subgroup of models, do not address the contributions due to variations in grip force. The above-described models can thus be considered valid in the vicinity of a selected grip force. Few investigators have proposed lumped-parameter models to account for variations in the grip force. Two different modelling approaches, based upon discrete and continuous variations in the grip force, have been considered. In the discrete modelling approach, different sets of model parameters are derived from the measured DPMI data corresponding to discrete levels of grip force, such that each set can be considered valid in the vicinity of the corresponding particular value of grip force. In the continuous modelling approach, the model parameters are identified as continuous functions of grip force, such that the DPMI response can be evaluated over a broader range of variations in grip force. Mishoe and Suggs [13] proposed three sets of model parameters, which were identified from measured DPMI data corresponding to 13, 27 and 40 N grip force. Reynolds and Falkenberg [14, 15] identified different sets of model parameters for 8·9, 25·4 and 35·6 N palm-type grip force. These studies retained the same structure of the three- and four-d.o.f. models, as illustrated in Figure 1(e) and 1(f).

Gurram [33, 36] proposed non-linear stiffness and damping characteristics for the three- and four-d.o.f. models to characterize the grip-force dependence of DPMI over a wide range of variation in grip force. The stiffness and damping coefficients were defined as proportional functions of grip force in the following manner:

$$k_i = k_{0i} + k_{Gi}F_{Gi}, \quad c_i = c_{0i} + C_{Gi}F_{Gi}, \quad i = 1, \ldots, n, \tag{9}$$

where k_i and c_i are stiffness and damping coefficients for the three- and four-d.o.f. models shown in Figures 1(e) and 1(f). k_{0i} and c_{0i} are constant stiffness and damping coefficients, and K_{Gi} and C_{Gi} are coefficients identified to account for mean grip force (F_G) dependent variations in stiffness and damping properties respectively. The impedance response of these models, corresponding to a particular grip force, can be evaluated from equations (6) and (7).

3. RELATIVE EVALUATIONS OF HAV MODELS

A total of 12 models are evaluated in a relative fashion in order to identify the models that could be applied to assess the vibration of power tools and to develop a mechanical simulator. These include the distributed-parameter model, and the 11 linear and grip-force-dependent lumped-parameter models, as described in the preceding section. The relative evaluations of grip-force-dependent models, however, are performed under a constant grip force in the vicinity of 25 N. The applicability of a mechanical-equivalent model in realizing a hand–arm simulator or coupled hand–tool analyses models, must satisfy three criteria: (1) the model should adequately describe the "to-the-hand" biodynamic response (magnitude and phase) of the hand and arm under vibration; (2) the deflections of model masses under a steady feed force must not be excessive in order to realize a feasible mechanical simulator; and (3) the model should describe important aspects of the vibration response of the human hand and arm, such as natural frequencies and damping ratios. The application of the last-cited criterion, however, poses difficulties, since there seems to be little quantitative knowledge on the vibration properties of the human hand and arm. This performance criterion is thus modified to include a qualitative analysis

of natural frequencies and damping ratios, such that the model frequencies lie within a reasonable frequency range with reasonable values of damping ratios.

The three criteria described above are used to evaluate the relative performance characteristics of the selected models. The first criterion is addressed by comparing the DPMI magnitude and phase response characteristics of selected models with the limits of most probable values defined in ISO-10068 [17]. For the second criterion, the equations of motion for the models are solved under a static feed force to derive the relative deflections of the contacting mass with respect to the fixed support, when included. In case of semi-definite system models, the relative deflections between extreme masses are evaluated. The resulting deflections associated with each model are examined within the context of a potential application of the model to the design of a mechanical simulator. The final criterion is based upon the free vibration characteristics of the models (natural frequencies and damping ratios) and their deviations from the range of frequencies considered in the particular study. The parameters of the reported models are summarized in Table 1 together with the essential information regarding the test conditions used, such as frequency range, grip force and magnitude of vibration (when reported). For studies involving different magnitudes of grip force, the model parameters are selected corresponding to the grip force that is closest to 25 N. These also included the models reported by Reynolds and Soedel [28], and Miwa *et al.* [30] for grip forces of 4·5–13·3 and 78·5 N respectively. The grip-force-dependent stiffness and damping parameters are considered for the three- and four-d.o.f. models reported by Gurram [33].

3.1. COMPARISON OF DPMI RESPONSE CHARACTERISTICS

Equations (3)–(8) are solved to derive DPMI magnitude and phase response characteristics of the selected models. The DPMI characteristics are compared with the upper and lower limits of DPMI response of the human hand and arm described in ISO-10068 [17], as illustrated in Figures 2–10. The results presented in Figure 3 suggest that the distributed-parameter model [26] underestimates the y_h-axis DPMI magnitude at frequencies above 45 Hz. The phase response of this model lies close within the suggested bounds at frequencies below 200 Hz and is considerably lower than the recommended lower limit at frequencies above 200 Hz. The two-stage, single-d.o.f. model [28] also yields an underestimate of the DPMI magnitude response along all the three axes in the majority of the frequency range, as shown in Figures 2–4. The DPMI phase responses of this model deviate considerably from the recommended bounds for all the three axes. The two-stage model also exhibits sharp discontinuities in the x_h-, y_h- and z_h-axis DPMI responses near 73, 40 and 100 Hz, respectively, which is more evident in the phase responses. These frequencies represent the transition frequencies of the two-stage models.

The y_h-axis magnitude response of the two-d.o.f. model proposed by Miwa [30] lies within the recommended bounds at frequencies below 330 Hz and exceeds the upper bound at higher frequencies (Figure 3). The corresponding phase response, however, lies outside the bounds in the majority of the frequency range. The model also yields considerably higher values of z_h-axis magnitude and phase response in the majority of the frequency range (Figure 4). Considerable deviations in the responses of these models [28, 30] from the recommended bounds may be partly attributed to consideration of considerably different magnitudes of grip forces in these studies (4·5–13·3 and 78·5 N respectively). The magnitude and phase response of the three-d.o.f. semi-definite system model proposed by Mishoe and Suggs [13] lies within the recommended bounds for x_h-axis over the entire frequency range (Figure 2). The y_h-axis magnitude response of this model, however, is slightly below the

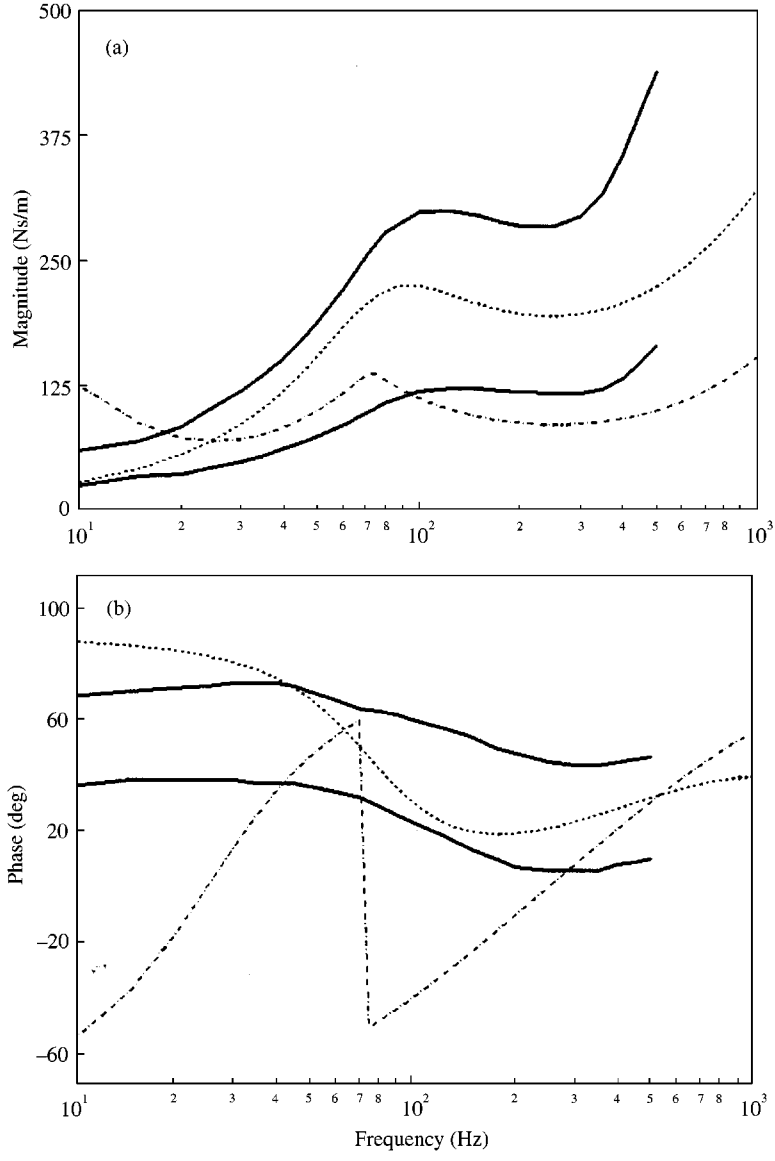

Figure 2. Comparison of DPMI responses of biodynamic models under x_h-axis vibration with range of idealized values: (a) magnitude; (b) phase (——, ISO limits; · · · · ·, Mishoe and Suggs [13]; and — · —, Reynolds and Soedel [28]).

lower bound at frequencies above 200 Hz (Figure 3). The three-d.o.f. system model with a fixed support, proposed for z_h-axis [13], also provides an underestimate of the magnitude response at frequencies above 23 Hz. The phase responses of these models are observed to be close to the recommended bounds in the majority of the frequency range. All of the above-mentioned models yield an extremely poor response for the z_h-axis in relation to the proposed bounds (Figure 4).

Figures 5–7 illustrate a comparison of x_h-, y_h- and z_h-axis DPMI responses, respectively, of the remaining three-d.o.f. models with a fixed support [12, 15, 17, 33] with respect to the recommended bounds. These models, with only few exceptions, yield comparable

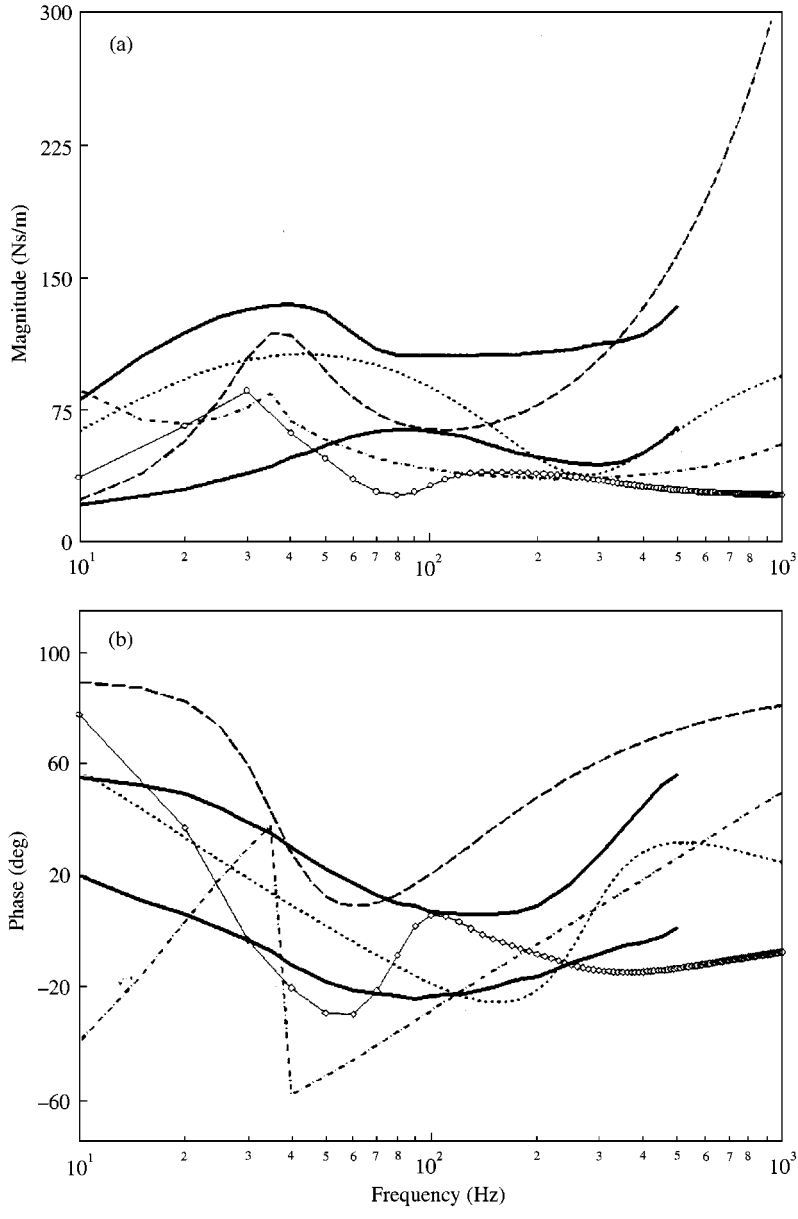

Figure 3. Comparison of DPMI responses of biodynamic models under y_h-axis vibration with range of idealized values: (a) magnitude; (b) phase (——, ISO limits; · · · · ·, Mishoe and Suggs [13]; —·—, Reynolds and Soedel [28]; – – –, Miwa *et al.* [30]; and —○—, Wood *et al.* [26]).

magnitude responses in the 20–500 Hz frequency range. The large deviations among the model responses at frequencies above 500 Hz are most likely attributed to extrapolations beyond the limited frequency range considered in some of the studies. The largest deviations between the models responses are again observed for the z_h-axis (Figure 7). The magnitude response of the model proposed by Daikoku and Ishikawa [17] lies within the recommended bounds for all three axes in the majority of the frequency range, except at low frequencies below 20–30 Hz. Although the model was formulated on the basis of data

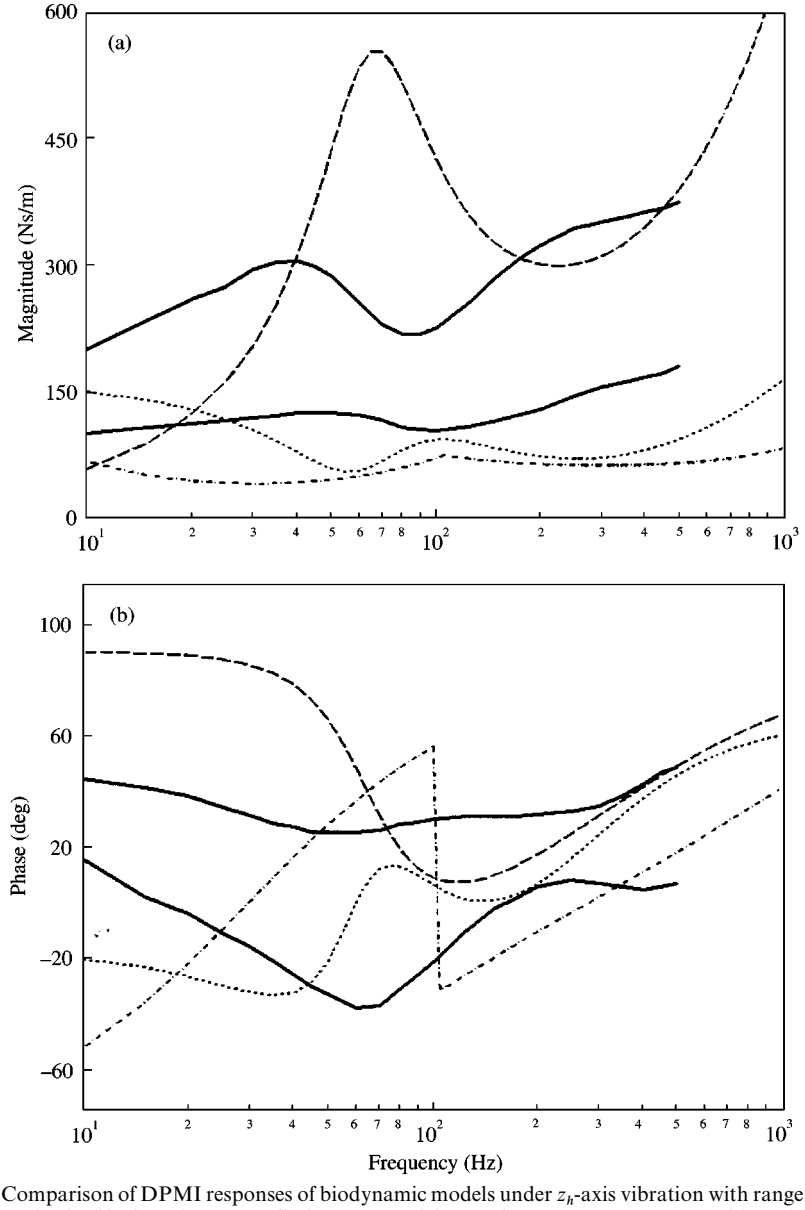

Figure 4. Comparison of DPMI responses of biodynamic models under z_h-axis vibration with range of idealized values: (a) magnitude; (b) phase (——, ISO limits; ·····, Mishoe and Suggs [13]; –·–, Reynolds and Soedel [28]; and – – –, Miwa *et al.* [30]).

acquired at frequencies up to 200 Hz, it yields reasonably good agreement with the bounds at frequencies above 22 Hz for the x_h-axis, in the 12–350 Hz range for y_h-axis and in the 22–400 Hz range for the z_h-axis. The phase responses of the models for the x_h- and z_h-axis, however, deviate considerably from the recommended bounds at frequencies below 70 Hz (Figures 5 and 6). The model proposed by Gurram [33] corresponding to a 25 N grip force yields reasonably good agreement with the recommended bounds for y_h- and z_h-axis up to 500 Hz (Figure 7). It should be noted that ISO-10068 [17] provides recommended limiting values only up to 500 Hz. The z_h-axis magnitude and phase responses, however, increase

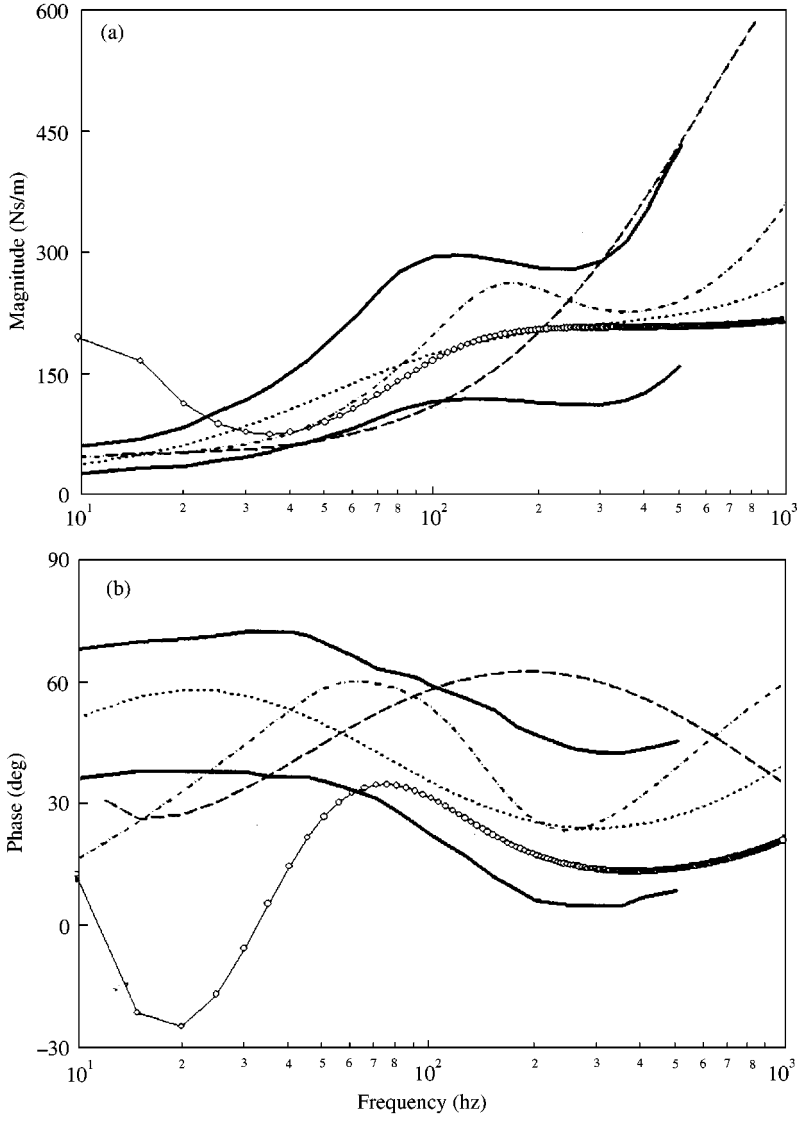

Figure 5. Comparison of DPMI responses of three-d.o.f. biodynamic models under x_h-axis vibration with range of idealized values: (a) magnitude; (b) phase (——, ISO limits; –·–, Reynolds and Falkenberg [14, 15]; – – –, Gurram [33]; ·····, ISO-10068 [17]; and —○—, Daikoku and Ishikawa [12]).

sharply at frequencies beyond 500 Hz. The x_h-axis magnitude response of Gurram's model also increases sharply at higher frequencies and exceeds the upper bound at frequencies above 300 Hz (Figure 5). The corresponding phase response lies outside the bounds in the 12–36 and 110–500 Hz bands.

The three-d.o.f. models proposed by Reynolds and Falkenberg [15] and ISO-10068 [17] yield best agreement with the recommended bounds for all three axes. Since the ISO models were formulated on the basis of the mean and ranges realized from a synthesis of large sets of data, the responses of these models are expected to lie within the bounds in the 10–500 Hz frequency range. The magnitude responses of the three-d.o.f. models proposed by Reynolds and Falkenberg [15] also lie within the recommended bounds for all three axes in the

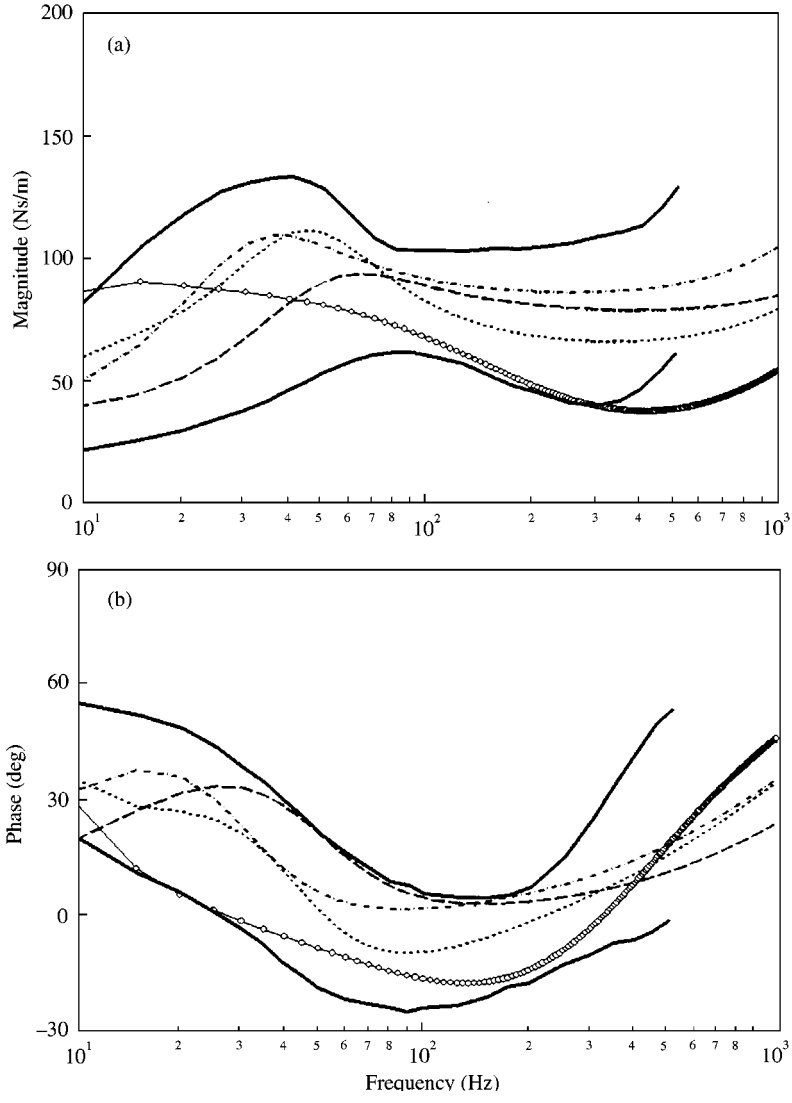

Figure 6. Comparison of DPMI responses of three-d.o.f. biodynamic models under y_h-axis vibration with range of idealized values: (a) magnitude; (b) phase (——, ISO limits; –·–, Reynolds and Falkenberg [14, 15]; – – –, Gurram [33]; ·····, ISO-10068 [17]; and —○—, Daikoku and Ishikawa [12]).

majority of the frequency range. The z_h-axis magnitude response, however, exceeds the upper bound at very low frequencies (below 18 Hz). The phase responses in the x_h- and z_h-axis also lie outside the corresponding bounds at low frequencies (Figures 5 and 7).

The DPMI magnitude responses of four-d.o.f. and beam models lie within the recommended bounds in the majority of the frequency range, as shown in Figures 8–10 for x_h-, y_h- and z_h-axis respectively. The model proposed by Gurram [33] exceeds the upper bound for z_h-axis in the 70–150 Hz band, as shown in Figure 10, and it yields considerably higher magnitudes in the x_h- and z_h-axis at frequencies above 500 Hz. The beam model [17] also yields a high magnitude response at higher frequencies along the x_h- and y_h-axis (Figures 8 and 9). The phase response of this model lies outside the bounds for the x_h- and

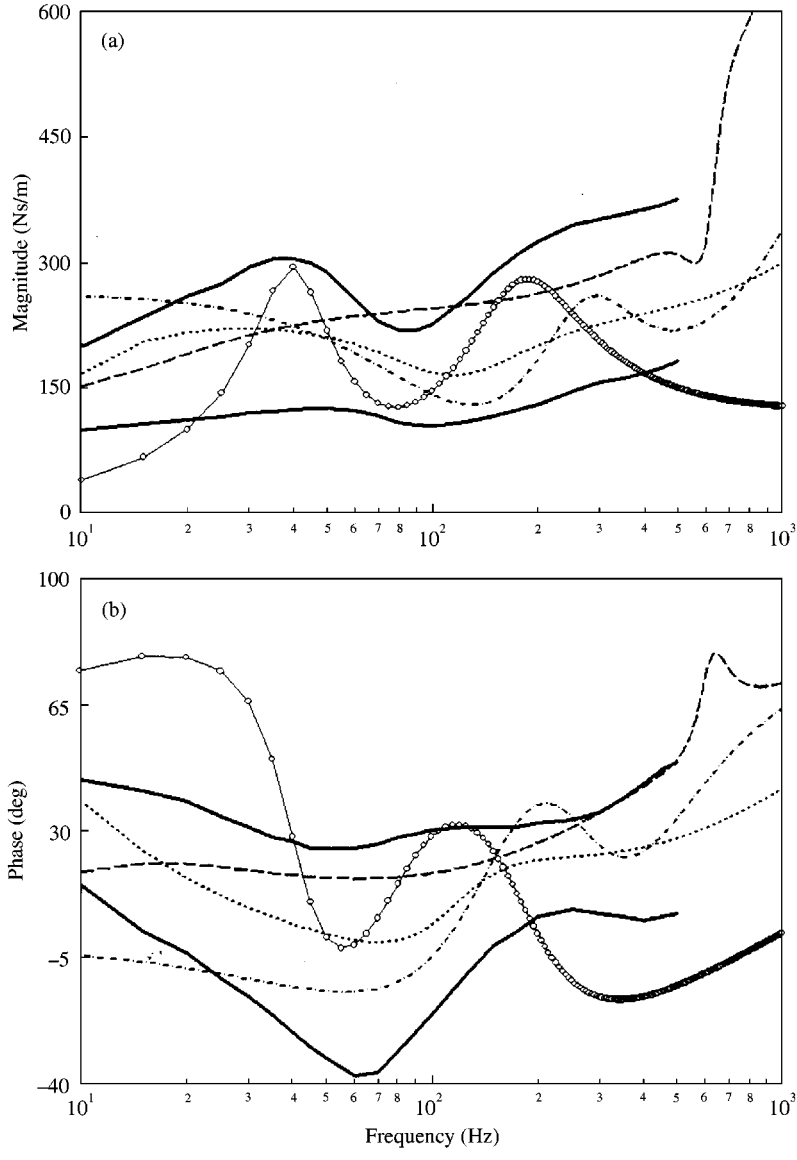

Figure 7. Comparison of DPMI responses of three-d.o.f. biodynamic models under z_h-axis vibration with range of idealized values: (a) magnitude; (b) phase (——, ISO limits; –·–, Reynolds and Falkenberg [14, 15]; – – –, Gurram [33]; ·····, ISO-10068 [17]; and —○—, Daikoku and Ishikawa [12]).

y_h-axis in most of the frequency range. The DPMI responses of the four-d.o.f. models proposed by Reynolds and Falkenberg [14], in general, lie within the recommended bounds with the exception of the z_h-axis phase response, which lies outside the bounds at frequencies below 20 Hz (Figure 10). The DPMI responses of the four-d.o.f. models proposed in ISO-10068 [17], as expected, lie well within the recommended bounds.

The comparison of the DPMI responses of the models suggests that higher order models, in general, yield better agreement with the ISO recommended limiting values of the biodynamic response of the human hand and arm. In view of the recommended limits of DPMI response, the three- and four-d.o.f. models proposed by Reynolds and Falkenberg

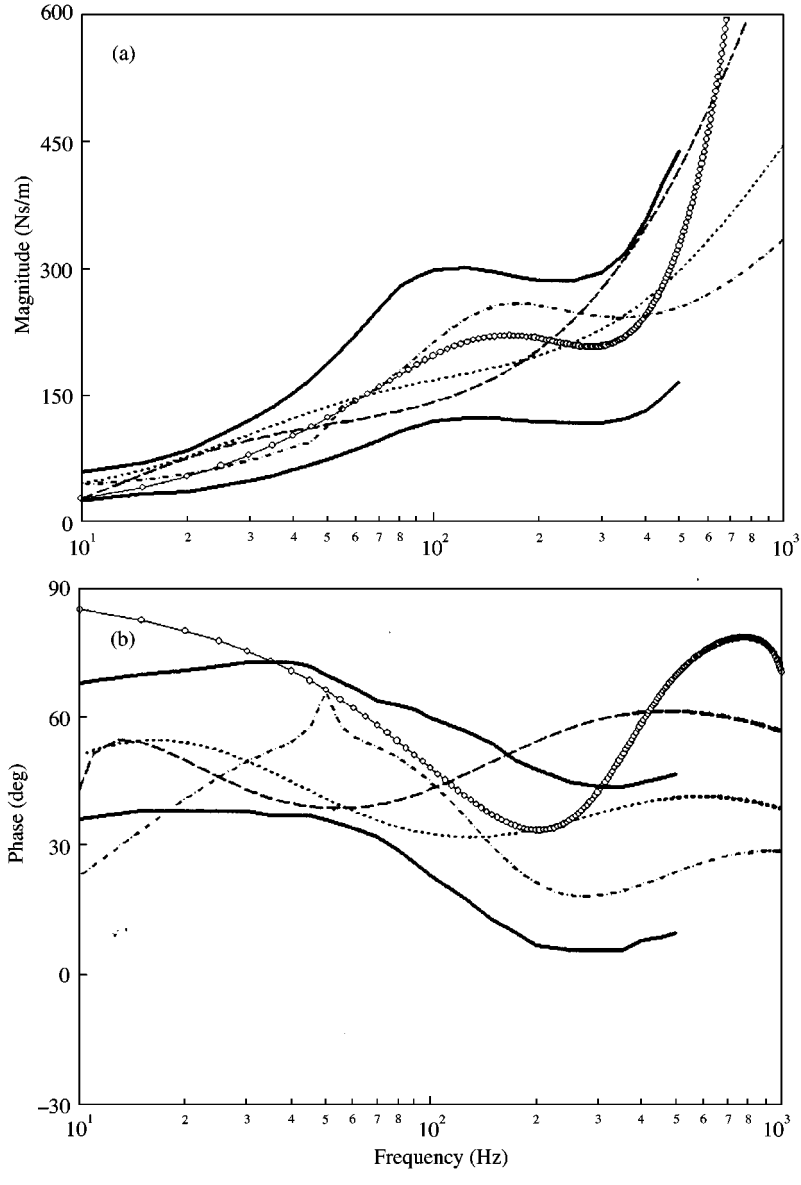

Figure 8. Comparison of DPMI responses of four-d.o.f. biodynamic models under x_h-axis vibration with range of idealized values: (a) magnitude; (b) phase (——, ISO limits; –·–, Reynolds and Falkenberg [14, 15]; – – –, Gurram [33]; ·····, ISO-10068 [17]; and —○—, ISO-beam model [17]).

[14, 15] and ISO-10068 [17] can be considered to provide the best agreement for all three axes. The two-d.o.f model of Mishoe and Suggs [13] also characterizes the biodynamic response adequately for x_h- and y_h-axis, while Daikoku's [12] three-d.o.f model can be considered appropriate for the y_h-axis alone. The three- and four-d.o.f. models proposed by Gurram [33] satisfy the recommended bounds for x_h- and y_h-axis, but yield a rapid increase in the x_h- and z_h-axis magnitude responses at frequencies above 500 Hz. On the basis of the DPMI response, the above-mentioned models appear to provide best agreement with the

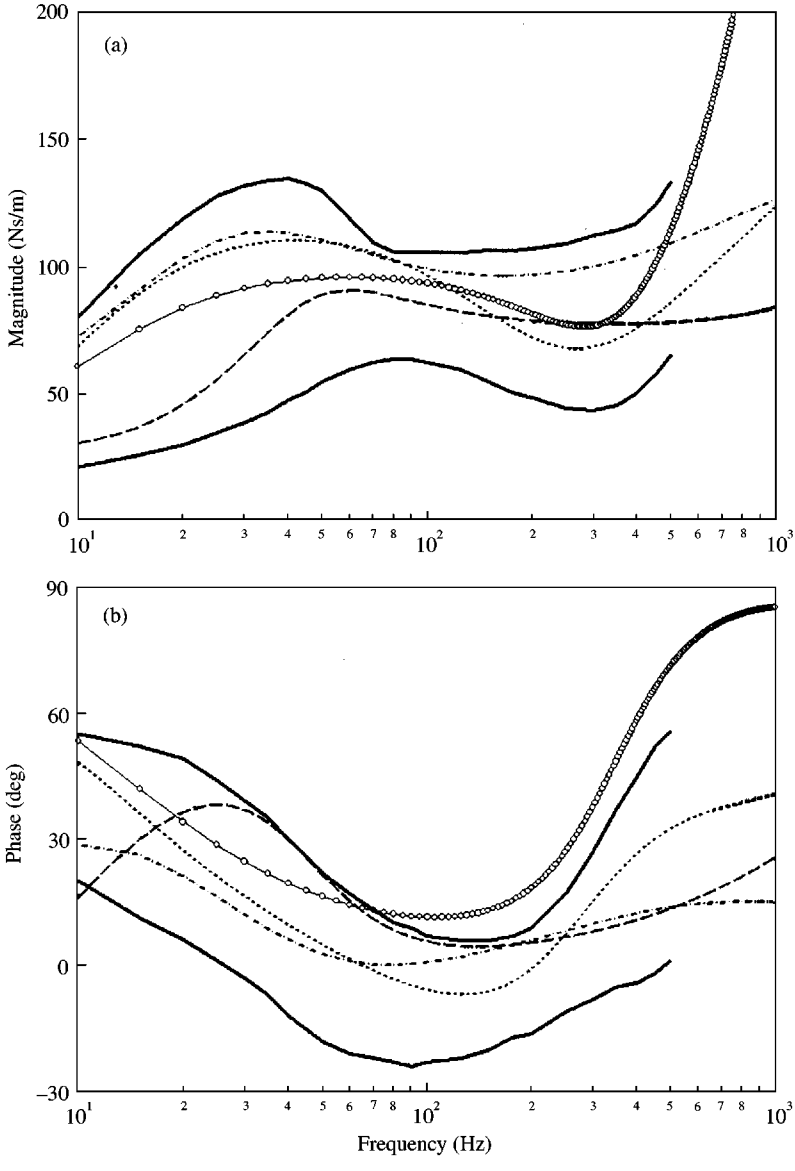

Figure 9. Comparison of DPMI responses of four-d.o.f. biodynamic models under y_h-axis vibration with range of idealized values: (a) magnitude; (b) phase (——, ISO limits; –·–, Reynolds and Falkenberg [14, 15]; – – –, Gurram [33]; ·····, ISO-10068 [17]; and —○—, ISO-beam model [17]).

range of idealized values proposed in ISO-10068 [17], and thus can be considered appropriate for the development of a mechanical simulator and studies on coupled hand–tool dynamic response.

3.2. NATURAL FREQUENCIES, DAMPING RATIOS AND OVERALL COMPLIANCE

Eigenvalue problems were formulated and solved to identify natural frequencies and damping ratios of the selected models [37]. The results, summarized in Table 2, are then

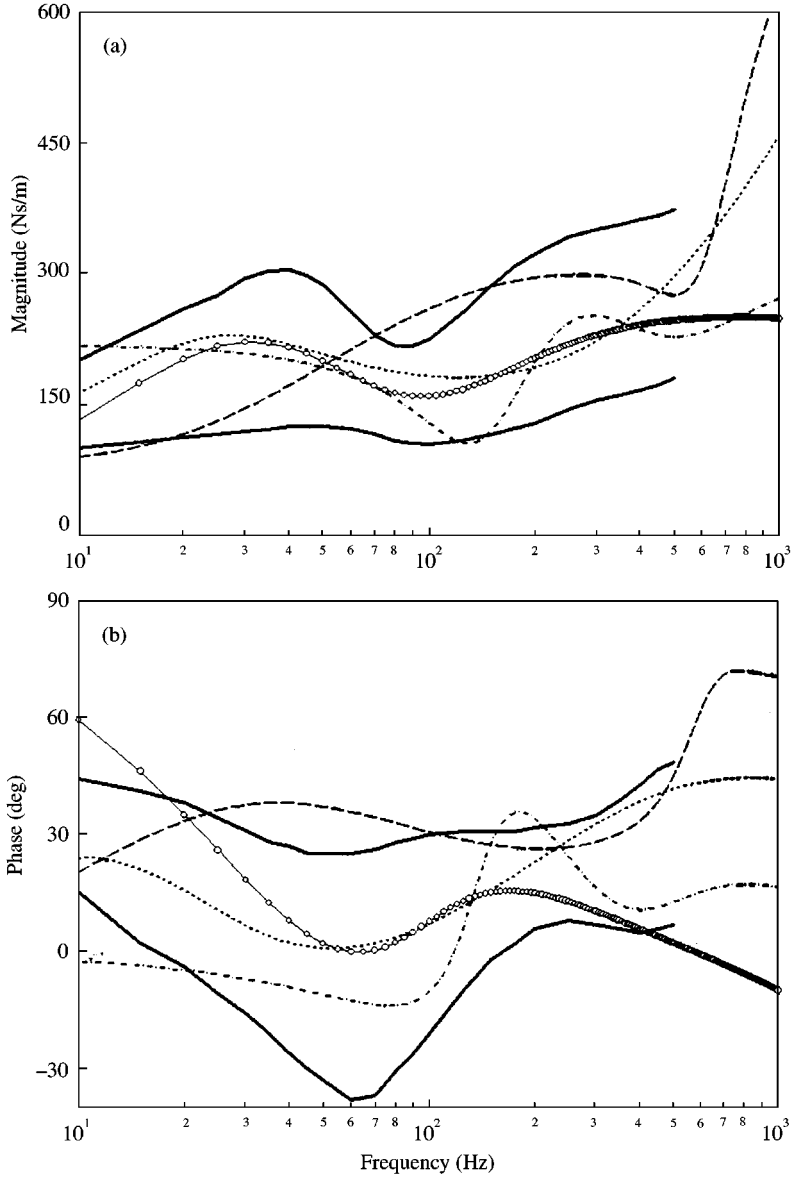

Figure 10. Comparison of DPMI responses of four-d.o.f. biodynamic models under z_h-axis vibration with range of idealized values: (a) magnitude; (b) phase (——, ISO limits; –·–, Reynolds and Falkenberg [14, 15]; – – –, Gurram [33]; ·····, ISO-10068 [17]; and —○—, ISO-beam model [17]).

examined to study their potential applicability to the development of models for coupled hand–tool analyses and mechanical hand–arm simulators. For the distributed-parameter model [26], a finite element analysis is performed to identify its natural frequencies, and only fundamental frequencies of the radius and ulna bones are reported. The eigenanalysis of the beam models reported in ISO-10068 [17] resulted in positive eigenvalues, thereby indicating instability; no attempts are therefore made to identify their natural frequencies and damping ratios. The overall compliance of each model is computed in terms of total static deflection (deflection of the driving point with respect to the fixed support or total

TABLE 2

Natural frequencies, damping ratios and static deflections of biodynamic models

Model	Natural frequencies (Hz)			Damping ratios			Deflection under 50 N force (mm)		
	x_h	y_h	z_h	x_h	y_h	z_h	x_h	y_h	z_h
Wood *et al.* [25]	—	13·3; 27·2	—	—	Distributed	—	—	1·1	—
Reynolds [27]									
(Stage I)	25·4	25·0	30·0	0·71	1·09	1·02	6·5	10·5	13·4
(Stage II)	249·5	228·6	280·9	1·25	1·73	1·87			
Miwa [29]	—	94·2	192·5		0·99	1·16	—	3·3	0·4
Mishoe [13]	216·1	94·2	45·9	1·42	0·38	0·33	4·6	28·1	34·0
	296·3	239·9	60·3	45·97	47·45	0·57			
			362·5			24·18			
Daikoku [12]	3·6	4·3	3·9	0·60	0·06	0·28	42·4	58·8	125·6
	33·5	41·2	75·0	0·60	0·59	0·48			
	462·4	576·2	1147·4	3·00	10·52	1·94			
Reynolds [15]—	4·1	2·9	4·6	3·36	1·86	334·44	285·7	289·0	285·7
three-d.o.f.	50·4	202·8	436·1	0·34	3·19	0·48			
	323·6	333·4	587·4	1·03	0·93	0·30			
Gurram [32]—	3·8	3·1	2·2	6·04	3·21	2·36	974·5	476·2	566·2
three-d.o.f.	9·1	62·7	5·2	0·03	2·90	42·31			
	46·8	320·8	635·8	1198·7	3·17	0·10			
ISO-10068 [17]—	2·4	4·4	4·2	1·39	2·85	0·16	423·7	176·0	28·6
three-d.o.f.	3·8	7·3	66·9	0·09	0·11	0·45			
	66·1	285·9	119·6	9·85	2·26	9·48			
Reynolds [15]—	3·5	1·7	3·2	2·68	1·71	1060·28	314·5	316·4	571·5
four-d.o.f.	50·3	71·3	49·7	0·06	0·44	283·29			
	157·0	149·5	469·8	150·90	42·29	0·57			
	345·9	172·4	711·9	1·02	1·53	0·98			
Gurram [32]—	5·5	6·3	2·7	12·66	1·24	2·94	271·7	112·3	197·6
four-d.o.f.	9·1	104·9	8·0	0·18	0·19	3·52			
	82·2	308·8	25·2	35·64	3·40	15·44			
	136·2	801·6	672·0	2·59	11·83	0·23			
ISO-10068 [17]—	1·9	2·1	2·4	1·62	10·77	1·55	546·4	204·1	276·2
four-d.o.f.	4·9	4·3	3·8	0·16	0·11	36·38			
	20·4	42·6	132·9	7·91	0·62	0·05			
	737·9	305·9	695·2	17·71	28·33	4·32			

deflection between the two extreme masses in case of semi-definite system models) under a constant feed force of 50 N. Although the feed force is known to vary considerably depending upon the individual factors, tool and operation, the selected value is based upon the value recommended in ISO-10819 [38]. The static deflection response of the distributed-parameter model is computed on the basis of stiffness elements (k_1 and k_2) representing soft tissue material of the hand in the vicinity of the tool handle. The computation of the static deflections associated with the beam model [17] were not attempted due to its unstable behavior, as determined from positive eigenvalues.

The resulting model deflections, also summarized in Table 2, describe the expected deflection of model masses if a mechanical simulator was to be realized on the basis of a particular model. Ideally, the static deflection should be relatively low, as expected from the total deflection of the skin and tissues in the human hand. It should be noted that the static deflection of the single-d.o.f. model [28] was computed using the parameters for the low-frequency (stage I) model. An examination of the results reveals that the reported models could experience deflections ranging from a low of 1·1 mm to a maximum of 974·5 mm under a 50 N static feed force. The higher order (three- and four-d.o.f.) models, in general, consist of elastic elements with relatively low stiffness and thus cause considerable deflections of the model masses. The three- and four-d.o.f. models [14, 15, 17, 33] suggest the use of very soft springs with stiffness ranging from 100 to 175 N/m. The beam model described in ISO-10068 suggests the use of springs with nearly zero stiffness. These models thus cause excessive deflections under the application of a static feed force. A mechanical equivalent model with high magnitude static deflection response would pose considerable difficulties in realizing a feasible mechanical simulator. The use of such a model with that of a hand-held power tool tends to yield highly asymmetric responses of the coupled hand–tool system [39]. The single-d.o.f. models [28] yield deflections ranging from 6·5 to 13·4 mm for all the three axes, while the two-d.o.f. model proposed by Miwa *et al.* [30] results in a peak deflection on the order of 3·3 mm for the y_h- and z_h-axis. The semi-definite three-d.o.f. model proposed by Mishoe and Suggs [13] also yields low deflection on the order of 4·6 mm for the x_h-axis. While these models may be considered more appropriate in view of reasonable deflections, their DPMI responses (with the exception of Mishoe's x_h-axis model) do not lie within the recommended bounds.

Furthermore, most of the higher order models suggest the use of extremely small masses, on the order of 1·2–1·8 g [14, 15, 33] and 4·3–4·5 g [12, 17]. The three-d.o.f. model proposed by Mishoe and Suggs [13] for y_h-axis suggests the use of a mass as low as 0·8 g. The models involving such small masses may be considered infeasible for the realization of a mechanical hand–arm simulator.

The natural frequencies of the biodynamic models of the human hand and arm tend to vary considerably as is evident from the results summarized in Table 2. Owing to the high dissipative properties of the human hand and arm, their natural frequencies are not clearly identifiable from the reported biodynamic response characteristics. All the three- and four-d.o.f. models, with the exception of that reported by Mishoe and Suggs [13] for the z_h-axis, yield either one or two low-frequency modes (well below 10 Hz), irrespective of the axis of vibration. Although the models reported by Reynolds and Falkenberg [14, 15] are formulated on the basis of measured data in the 5–1000 Hz frequency range, they exhibit lower modes in the 1·7–4·7 Hz frequency range. The models reported by Gurram [33] and ISO-10068 [17], in a similar manner, exhibit lower modes in the 1·9–9·1 Hz range, while they are derived from the biodynamic response data at frequencies above 10 Hz. The four-d.o.f. ISO-model also results in higher modes at frequencies (695·2 and 737·9 Hz) well above its upper limit of 500 Hz. In a similar manner, the natural frequencies of the models reported by Daikoku and Ishikawa [12] lie well below the lower limit of 8 Hz and well

above the upper limit of 200 Hz considered in their study. The existence of low-frequency modes is attributed to elastic elements with relatively low stiffness, which tend to cause excessive static deflections.

While there is no agreement among the reported models in terms of the natural frequencies of the human hand and arm, the models suggest the existence of natural frequencies in the 20–50 and 60–82 Hz bands for all three axes, the 120–160 Hz band for the x_h- and z_h-axis, and the 150–172 Hz band for the y_h-axis, and the 200–300 Hz band for the x_h- and y_h-axis. This lack of agreement has also been reported by Gurram *et al.* [16] on the basis of measured biodynamic responses of the human hand and arm reported in the literature. It was reported that the majority of the impedance magnitude data reveals peaks in the 100–200 and 30–100 Hz bands in the x_h- and y_h-axis, and in the 20–50 Hz band and near 300 Hz in the z_h-axis. The biodynamic models also yield wide variations in damping ratios associated with different modes of vibration. The damping ratios of the selected models vary from a low of 0·06 to a high of 1060. While the knowledge of dissipative properties of the human hand and arm does not yet exist to enable quantitative comparisons, the models with relatively high damping ratios would pose difficulties in realizing a mechanical hand–arm simulator.

3.3. DISCUSSIONS ON POTENTIAL APPLICATIONS OF MODELS

The results of the comparisons of the response characteristics of the mechanical equivalent models of the human hand and arm in terms of their DPMI response and compliance raise many doubts regarding the potential applicability of these models for the development of mechanical simulators or coupled hand–tool analysis models. While models based upon three- or four-d.o.f. structures yield biodynamic responses that are generally agreeable with the limits prescribed in ISO-10068 [17], these models consist of relatively low masses and restoring elements with low stiffness. These models, therefore, exhibit low-frequency natural modes (below 10 Hz) and excessive static deflections under a steady feed force, which argue against their potential application. In view of their compliances or static deflections under a 50 N feed force, the models that could be considered suitable include: the three-d.o.f. model proposed by Mishoe and Suggs [13] for the x_h-axis (deflection = 4·6 mm); the two-d.o.f. models of Miwa *et al.* [30] for the y_h- and z_h-axis (deflections = 0·4 and 3·3 mm); the two-stage single-d.o.f. models proposed by Reynolds and Soedel [28] for all three axes (peak deflection = 13·4 mm); and the distributed parameter model of Wood *et al.* [26] for the y_h-axis with a deflection of 1·1 mm of the skin and soft tissues within the hand. The potential application of the two-stage models to the design of a mechanical simulator, however, would pose practical difficulties. These models, with the exception of that proposed by Mishoe and Suggs [13] for the x_h-axis alone, fail to characterize the DPMI response of the human hand and arm within the recommended bounds. This model [13] alone thus satisfies the requirements involving characterization of the DPMI response and the static deflection.

The natural frequencies identified from either the models or the reported measured data raise further concerns on the potential applications of both the data and the models. The natural frequencies of the human hand and arm are not clearly identifiable from the reported data, although relatively wide ranges have been suggested [16]. Both the measured data and the models show very little agreement regarding the peak magnitudes and their corresponding frequencies. This may be attributed to wide variations in both the test conditions, and measurement and analyses methods employed. Consequently, very little knowledge exists on the natural frequencies and dissipative properties of human hand and arm. The ISO-10068 [17] presents relatively wide ranges of DPMI responses that have been

derived from the synthesis of broadly different data reported by different investigators. It is thus highly desirable to undertake additional measurements of the biodynamic response of the human hand–arm system under carefully defined ranges of test conditions, such as grip force, feed force, posture, and magnitude and frequency of vibration excitation. Modern measurement methods, such as scanning laser Doppler vibrometers, ultrasonic sensors and infrared cameras should be employed to clearly identify resonant frequencies and modal behavior of the human hand and arm. These measurement systems could also be used to study the transmission of vibration to different segments of the hand and arm.

The higher order models, in general, yield either one or two modes at frequencies well below 10 Hz, as illustrated in Table 2. A model structure with fewer d.o.f. may thus be attempted with appropriate consideration of the DPMI response and model compliance. The model parameter identification tasks should involve adequate limit constraints on the static deflection of model masses and dissipative properties of the human hand and arm, while further studies on identification of these limits are highly desirable.

4. CONCLUSIONS

Owing to the severe health effects of prolonged exposure to hand-transmitted vibration from operation of power tools, it is essential to characterize and assess the vibration from different tools in an efficient manner, and to develop efficient analytical tools for designing and assessing vibration attenuation mechanisms. The 12 reported mechanical equivalent models of the hand and arm system are evaluated in an attempt to identify a suitable model that could (a) form the basis for the development of a mechanical hand–arm simulator to enable efficient and consistent relative evaluations of different tools to be done in the laboratory, and (b) support the analysis and assessment of anti-vibration power tools and protective devices through development of coupled hand–tool analysis models. The evaluations are performed using a performance criteria comprising the recommended ranges of driving-point mechanical impedance characteristics of the human hand and arm, model deflection under a steady feed force and vibration properties of the human hand and arm. The models are initially evaluated in terms of their ability to characterize the DPMI response of the human hand and arm. The static deflections of the models under a known feed force of 50 N are then examined from the perspective of their applicability to the design of a mechanical hand–arm simulator. The natural frequencies and damping ratios of various models are finally evaluated and compared relative to known ranges of predominant frequencies from the available DPMI data. From a comparison of the DPMI responses to the limiting values proposed in ISO-10068, it is concluded that three- and four-d.o.f. models, in general, yield acceptable characterizations of the biodynamic response of the human hand and arm. The DPMI responses of the distributed-parameter, and single- and two-d.o.f. lumped-parameter models lie outside the ISO-recommended limits. The model parameters in the majority of the studies are identified by fitting the target DPMI response functions in a specified frequency range (usually above 10 Hz), while the resulting modal properties and responses to a steady feed force are ignored. The majority of the higher order models thus exhibit either one or two modes at considerably lower frequencies, below 10 Hz. These models invariably consist of very light masses and elastic elements with low stiffness, and thus yield excessive deflections under application of a steady feed force. The low natural frequency modes and resulting high deflections of these models make it inappropriate to apply them to the design and development of a mechanical hand–arm simulator. These models also yield high damping ratios, which may deter their potential application. The current state of knowledge on the vibration behavior of the human

hand–arm system does not permit a quantitative evaluation of the models in terms of their natural frequencies and dissipative properties. It is thus vital to undertake further studies using modern measurement methods.

REFERENCES

1. G. GEMME and W. TAYLOR 1983 *Journal of Low Frequency Noise and Vibration, Special Volume*: 1–12. Foreword: hand–arm vibration and the central autonomic nervous system.
2. P. L. PELMEAR and D. E. WASSERMAN 1998 *Hand–Arm Vibration—a Comprehensive Guide for Occupational Health Professionals*. Beverly Farms, MA: OEM Press.
3. M. J. GRIFFIN 1990 *Handbook of Human Vibration*. London: Academic Press.
4. ISO 5349-1 2000 Mechanical vibration—measurement and evaluation of human exposure to hand-transmitted vibration. Part 1: general guidelines.
5. M. BOVENZI 1998 *International Archives of Occupation and Environmental Health* **71**, 509–519. Exposure–response relationship in the hand–arm vibration syndrome: an overview of current epidemiology research.
6. B. P. KATTEL and J. E. FERNANDEZ 1999 *International Journal of Industrial Ergonomics* **23**, 595–608. The effects of rivet gun on hand–arm vibration.
7. ISO/DIS 5349 1999 Mechanical vibration—measurement and evaluation of human exposure to hand-transmitted vibration. Part 2: practical guidance for measurement in the workplace.
8. ISO 8662 Parts 1–14 1991 Hand-held portable power tools—measurement of vibrations at the handle.
9. J. KINNE and R. MELZIG-THIEL 1996 *Central European Journal of Public Health* **40**, 53–56. Derivation of mean impedance curves as a basis for mechanical models of the human hand–arm system.
10. R. JAHN and M. HESSE 1986 *Scandinavian Journal of Work, Environment & Health* **12**, 343–346. Applications of hand–arm models in the investigation of the interaction between man and machine.
11. H.-J. BULLINGER, W. F. MUNTZINGER and P. LAUSTER 1989 in *Advances in Industrial Ergonomics & Safety I* (A. Mital (editor), 575–582. London: Taylor & Francis. Numeric simulation of hand-transmitted vibrations.
12. M. DAIKOKU and F. ISHIKAWA 1990 *Proceedings of Fifth International Conference on Hand–Arm Vibration. Kanzawa, Japan*. Mechanical impedance and vibration model of hand–arm system.
13. J. W. MISHOE and C. W. SUGGS 1977 *Journal of Sound and Vibration* **53**, 545–558. Hand–arm vibration. Part II. Vibrational responses of the human hand.
14. D. D. REYNOLDS and R. J. FALKENBERG 1984 *Journal of Sound and Vibration* **95**, 499–514. A study of hand vibration on chipping and grinding operators. Part II: four-degree-of-freedom lumped parameter model of the vibration response of the human hand.
15. D. D. REYNOLDS and R. J. FALKENBERG 1982 in *Vibration Effects on the Hand and Arm in Industry*. (A. J. Brammer and W. Taylor, editors), 117–132. Three- and four-degrees of freedom models of the vibration response of the human hand.
16. R. GURRAM, S. RAKHEJA and A. J. BRAMMER 1995 *Journal of Sound and Vibration* **180**, 437–458. Driving-point mechanical impedance of the human hand–arm system: synthesis and model development.
17. ISO-10068 1998 Mechanical vibration and shock—free, mechanical impedance of the human hand–arm system at the driving point.
18. C. H. LEWIS 2000 *Proceedings of 35th UK Group Meeting on Human Responses to Vibration, Southampton, England*, 249–259. Evaluating the vibration isolation of soft seats using an active anthropodynamic dummy.
19. P.-É. BOILEAU, S. RAKHEJA, X. YANG and I. STIHARU 1997 *Noise and Vibration Worldwide* **28**, 7–15. Comparison of biodynamic response characteristics of various human body models as applied to seated vehicle drivers.
20. C. W. SUGGS, L. F. STIKELEATHER, J. Y. HARRISON and R. E. YOUNG 1970 *Transactions of the American Society of Agricultural Engineering* **13**, 378–381. Application of a dynamic simulator in seat testing.
21. S. RAKHEJA, R. GURRAM and G. J. GOUW 1993 *Journal of Biomechanics* **26**, 1253–1260. Development of linear and nonlinear hav models using optimization and linearization techniques.

22. D. D. REYNOLDS and E. N. ANGEVINE 1977 *Journal of Sound and Vibration* **51**, 255–265. Hand–arm vibration. Part II: vibration transmission characteristics of the hand and arm.
23. T. CHERIAN, S. RAKHEJA and R. B. BHAT 1996 *International Journal of Industrial Ergonomics* **17**, 455–467. An analytical investigation of an energy flow divider to attenuate hand-transmitted vibration.
24. M. FRITZ 1991 *Journal of Biomechanics* **21**, 1165–1171. An improved biomechanical model for simulating the strain of the hand–arm system under vibration stress.
25. ISO-8727 1997. Mechanical vibration and shock—human exposure—biodynamic coordinate systems. International Standard Organization.
26. L. A. WOOD, C. W. SUGGS and C. F. ABRAMS 1978 *Journal of Sound and Vibration* **57**, 157–169. Hand–arm vibration. Part III: A distributed parameter dynamic model of the human hand–arm system.
27. D. DIECKMANN 1958 *Internationale Zeitschrift Angewandter Physiologie Einschließlicher Arbeitsphysiologie* **17**, 125–132. Ein mechanisches modell für das schwingungserregte hand–arm system des menschen.
28. D. D. REYNOLDS and W. SOEDEL 1972 *Journal of Sound and Vibration* **21,** 339–353. Dynamic response of the hand–arm system to a sinusoidal input.
29. C. F. ABRAMS 1971 *Ph.D. Thesis, North Carolina State Universit*. Modeling the vibrational characteristics of the human hand by the driving point mechanical impedance method.
30. T. MIWA, Y. YONEKAWA, A. NARA, K. KANADA and K. BABA 1979 *Industrial Health* **17**, 85–122. Vibration isolators for portable vibrating tool. Part 1. A grinder.
31. G. MELTZER 1979 *Proceedings of the International Symposium on Man under Vibration Suffering and Protection, Udine, Italy*, 210–221. A vibration model for the human hand–arm system.
32. R. GURRAM, S. RAKHEJA and G. J. GOUW 1995 *International Journal of Industrial Ergonomics* **16**, 135–145. Biodynamic response of the human hand–arm system subject to sinusoidal and stochastic excitations.
33. R. GURRAM 1993 *Ph.D. Thesis, Concordia University, Montreal*. A study of vibration response characteristics of the human hand–arm system.
34. L. BURSTROM 1990 *International Archives of Occupation and Environ Health* **62**, 431–439. Measurement of the impedance of the hand and arm.
35. R. LUNDSTROM and L. BURSTROM 1989 *International Journal of Industrial Ergonomics* **3**, 235–242. Mechanical impedance of the human hand–arm system.
36. R. GURRAM, S. RAKHEJA, P.-E. BOILEAU and G. J. GOUW 1996 *Central European Journal of Public Health* **40**, 65–68. Development of a grip force dependent hand–arm vibration model.
37. C. M. HARRIS 1995 *Shock and Vibration Handbook*. New York, NY: McGraw-Hill; fourth edition.
38. ISO-10819 1996 Mechanical vibration and shock—hand–arm vibration–method for the measurement of the vibration transmissibility of gloves at the palm of the hand.
39. C. RAJALINGHAM, S. RAKHEJA and P.-É. BOILEAU 2000 *Report CONCAVE* 01-00, *Concordia University, Montreal*. Vibration analysis of a hand-held percussive tool: model development and validation.

APPENDIX A: DERIVATION FOR DPMI OF THE DISTRIBUTED-PARAMETER MODEL [26]

The model shown in Figure 1(a) can be considered as two independent mass–spring–beam systems. Owing to the boundary conditions defined for the model, the total driving-point mechanical impedance of the model is derived as the sum of DPMI of two independent beams. First, a matrix of four pole parameters for each system, which relates the input and output of forces and velocities, can be calculated using the equation

$$\begin{bmatrix} \eta_{11} & \eta_{12} \\ \eta_{21} & \eta_{22} \end{bmatrix}_i = [M]_i[S]_i[\alpha]_i, \quad i = 1, 2, \tag{A.1}$$

where

$$[M]_i = \begin{bmatrix} 1 & \mathrm{j}\omega m_i \\ 0 & 1 \end{bmatrix}, \quad [S]_i = \begin{bmatrix} 1 & 0 \\ c_i + k_i/\mathrm{j}\omega & 1 \end{bmatrix}$$

$$[\alpha]_i = \frac{-1}{\sinh \beta_i L - \sin \beta_i L}$$

$$\times \begin{bmatrix} \sin \beta_i L \cos \beta_i L - \sinh \beta_i L \cos \beta_i L & \dfrac{-\beta_i^3 EI_i^*}{j\omega}(1 - \cosh \beta_i L \cos \beta_i L) \\ \dfrac{-j2\omega}{\beta_i^3 EI_i^*} \sinh \beta_i L \sin \beta_i L & \sin \beta_i L \cos \beta_i L - \sinh \beta_i L \cos \beta_i L \end{bmatrix} \quad \text{(A.2)}$$

in which

$$\beta_i = \left[\frac{\rho_i \omega^2}{EI_i^*}\right]^{1/4}, \quad L_1 = L_2 = L \quad \text{and} \quad EI_i^* = EI_i\left(1 + j2\xi_i \frac{\omega}{\omega_{1r}}\right), \quad i = 1, 2. \quad \text{(A.3)}$$

The total driving-point impedance of the model is then computed from those of the beams, derived from equations (A.1)–(A.3) [26]:

$$Z(j\omega) = \frac{F_A(j\omega)}{\dot{q}_A(j\omega)} = \left[\frac{\eta_{11}}{\eta_{21}}\right]_{i=1} + \left[\frac{\eta_{11}}{\eta_{21}}\right]_{i=2}. \quad \text{(A.4)}$$